Cite as: Abarca-Ortega A, González-Bermúdez B, Plaza GR, Enhancing micropipette aspiration with artificial-intelligence analysis, Biophysical Journal, Volume 123, Issue 17, 2024, Pages 2860-2868,ISSN 0006-3495, DOI: https://doi.org/10.1016/j.bpj.2024.04.006.

Article

Enhancing Micropipette Aspiration with Artificial-Intelligence Analysis

Aldo Abarca-Ortega[1,2,3*], Blanca González-Bermúdez[2,3,4], and Gustavo R. Plaza[2,3,4*]

[1]Departamento de Ingeniería Mecánica, Universidad de Santiago de Chile, USACH, Santiago de Chile, Chile
[2]Departamento de Ciencia de Materiales, ETSI de Caminos, Universidad Politécnica de Madrid, E-28040 Madrid, Spain
[3]Centro de Tecnología Biomédica, Universidad Politécnica de Madrid, E-28223 Pozuelo de Alracón, Spain
[4]Instituto de Investigación Sanitaria Hospital Clínico San Carlos, IdISSC, Madrid, Spain
[*]Correspondence: aldo.abarca@ctb.upm.es, gustavo.plaza@upm.es

ABSTRACT The micropipette aspiration technique is commonly used in the field of mechanobiology, offering a a variety of measurement types. To extract biophysical parameters from the experiments, numerical analysis is required. Although previous works have developed techniques for the partial automation of this analyses, these approaches are relatively time-consuming for the researchers. In this article we describe the development and application of an artificial-intelligence tool for the completely-automatic analysis of micropipette aspiration experiments. The use of this tool is compared with previous methods and the impressive reduction in the time required for these analyses is discussed. The new tool open new possibilities for the micropipette aspiration technique by enabling dealing with large numbers of experiments and real-time measurements.

SIGNIFICANCE This article presents the creation and utilization of an artificial-intelligence tool for analyzing micropipette aspiration experiments. This innovation enables novel applications and significantly reduces the time needed for researchers to evaluate biophysical parameters.

INTRODUCTION

Cell biophysics bridges the realms of physics and biology by applying established physical methodologies and tools to investigate the intricate world of living cells. This multidisciplinary field intersects with various disciplines, including molecular biology, biochemistry, and bioengineering. Biophysical properties, particularly mechanical properties, are useful biomarkers of cell state (1), as they are related to cell components. One crucial aspect involves using experimental techniques to quantify pertinent parameters accurately. Borrowing extensively from materials science, cell biophysics adapts its methodologies to unravel the mysteries of living matter. For instance, when studying mechanical properties, commonly employed phenomenological approaches harnessed in materials science are often adopted to characterize the behaviors of cells and tissues. These approaches treat the material as a continuum medium defined by a concise set of parameters, being the assessment of the Young's modulus a paramount example.

A variety of experimental techniques have been adapted or developed to measure biophysical parameters, particularly mechanical parameters. Most of these techniques make use of microsized probes, and the force is applied by either mechanical, optical or magnetic systems (2). These tools have provided valuable knowledge on cell internal ordering, function and mechanical properties, indicating that changes in the mechanical properties of cells are linked to a variety of biological processes (3). Moreover, measurements of cell mechanical properties do not require extrinsic labels, such as fluorescent markers, and hence constitute suitable biomarkers for cell characterization. A major weakness of the classical methods of the field concerns the technically demanding and time-consuming procedures (4). Although new microfluidics-based approaches have been recently developed (5), these techniques require also trained operators and are relatively time-consuming.

The micropipette-aspiration technique was developed in the 1950s (6). The technique has been extensively used to assess mainly mechanical parameters of cells and tissues (7), being a useful auxiliary technique for cell manipulation (8). Part of the

Cite as: Abarca-Ortega A, González-Bermúdez B, Plaza GR, Enhancing micropipette aspiration with artificial-intelligence analysis, Biophysical Journal, Volume 123, Issue 17, 2024, Pages 2860-2868,ISSN 0006-3495, DOI: https://doi.org/10.1016/j.bpj.2024.04.006.

success of the technique is due to the simplicity of the setup required to perform experiments: basically, a microcapillary is used to aspirate the sample, by using a lower pressure inside the capillary than the pressure in the liquid medium containing the cell. This differential pressure may be obtained simply by connecting the microcapillary to a water reservoir whose height may be adjusted manually or electromechanically (9). The aspiration of the sample is observed in a microscope, and the acquired images are analyzed to quantify biophysical parameters, in particular mechanical parameters.

Determining mechanical parameters for cells or tissues subjected to micropipette aspiration relies on employing mechanical models. A straightforward approach involves treating the sample as a homogeneous isotropic material. In this context, the model developed by Theret et al., which considers the sample to be a semi-space, is a commonly used reference (10). However, as we have extensively discussed in our prior research (7, 11, 12), a notable limitation of this model is its failure to account for the impact of the finite size of suspended cells. To address this limitation, we propose the adoption of a linearized equation (11) derived from the numerical model pioneered by Zhou et al. (13). It is worth noting that all these models necessitate an assessment of the dimensions of the cells undergoing aspiration, a task commonly accomplished by analyzing microscopy images captured during the aspiration process. In particular, the initial size of the cell (initial diameter of the unloaded cell) and the progressive displacement of the cell front during the aspiration process are required (11).

The technique has undergone significant evolution over the decades, witnessing substantial advancements in practical application and a gradual shift toward partial automation of the analysis (7, 12). A recent advance consisted of using laser interferometry to measure the front-cell displacement during the aspiration process (14), allowing for precise estimation of mechanical parameters, including dynamical loading. In that work, the application of the technique was demonstrated for relatively large cells. In the case of cells with a size of the order of ten microns, the conventional procedure to measure the displacement of the cell front during the loading process is based on digital measurements on the microscopic images acquired during the experiments (11). The degree of automation in the analysis process hinges on the active involvement of the researcher for accurate cell feature identification, a crucial step to derive digital measurements essential for quantifying the parameters of interest. The most straightforward method for digital measurements involves a picture-by-picture analysis performed by the researcher using suitable software. A better, relatively simple, approach for the digital analysis of the images in order to compute cell-front displacements consist of programming the software to detect the cell front based on changes in pixel intensity (12, 15). This approach requires the active participation of the researcher in order to select the appropriate region of interest in the pictures and to detect artifacts. To eliminate the researcher's active involvement and introduce a new level of objectivity into the analysis, this work introduces a novel approach based on artificial intelligence (AI) tools. This innovation results in a fully automated and robust analysis of experiments, effectively eliminating any subjective elements introduced by human intervention.

In this work, we have demonstrated the practical application of the novel tool by studying the mechanical properties of living T cells. T cells play a pivotal role in immune responses, with their migration to infection sites being indispensable for combating pathogens. Moreover, T cells are crucially involved in the gradual decline in immune function associated with aging. Thus, progress toward the overarching goal of promoting healthy aging implies enhancing the functionality of the elderly immune system, particularly the efficacy of immune cells. In a previous study, we identified a relationship between a reduced migration and higher cell stiffness (15). Despite the available knowledge of these features, the understanding of how mechanics, structure, and functions are connected is incomplete (16). Thus, in order to enhance the study of biophysical properties of T cells, it is of interest developing experimental and analytical tools to accelerate the computation of biophysical parameters in order to facilitate dealing with large numbers of experiments.

MATERIALS AND METHODS

In this section, we present the methods used to develop and validate the AI tool for object recognition. Our focus is on applying convolutional neural networks (CNNs) for accurate and automated identification of cell boundaries in micropipette aspiration assays. In the following subsections we describe the mechanical model, the training and configuration of our neural network, image data extraction and mechanical assessments. In this work, 15 experiments of T cells were randomly selected from previously conducted experiments (12).

Cite as: Abarca-Ortega A, González-Bermúdez B, Plaza GR, Enhancing micropipette aspiration with artificial-intelligence analysis, Biophysical Journal, Volume 123, Issue 17, 2024, Pages 2860-2868,ISSN 0006-3495, DOI: https://doi.org/10.1016/j.bpj.2024.04.006.

Mechanical model

The micropipette aspiration technique requires the accurate measurement of cell deformation through microscopic image analysis. The basic operation of the technique involves applying a differential pressure (ΔP) through a micropipette typically with an internal diameter similar (and smaller) to that of the cells. The standard setup entails controlling the vertical movement of a water reservoir to generate aspiration pressure ΔP, calculated as $\rho g h$ (where h is the height of the free surface of the reservoir and ρg is the specific weight of the water). The most widely accepted and used models assume incompressibility and linear elastic behavior of the cell for small deformations. As discussed elsewhere (7, 12), the Plaza et al.'s linearized model (11), based on a previous model by Zhou et al. (13), is appropriate to analyze the experiments assuming homogeneous, isotropic, elastic, incompressible cell, and provides the equation

$$\frac{\Delta P}{E} = c_l \frac{L_p}{R_p}, \qquad (1)$$

where c_l is a variable that accounts for the relative size of the cell to the pipette, determined as $c_l = (\beta_1/3)\,[1 - (R_p/R_c)^{\beta_3}]$ (11). In these equations, ΔP is the differential aspiration pressure, E is the apparent Young's modulus, L_p is the aspirated length (the distance the front of the cell advances inside the micropipette), and R_p is the internal radius of the micropipette. Constants β_1 and β_3, with values of 2.0142 and 2.1187 respectively (11, 13). Linear fitting of the equation, in order to obtain Young's elastic modulus E at small deformations, is performed in the normalized aspirated range $0.1 < L_p/R_p < 0.3$ (7, 11, 12).

Identification of cells in the microscopy images

In this study, we developed an image analysis software for micropipette aspiration assays AI object recognition tools. The primary objective was to create a convolutional neural network (CNN) that is generalizable, automatic, and user-friendly. The CNN was trained and validated using a dataset comprising 239 images from previous experiments, capturing various states of cell aspiration. These images, both raw and processed from previous analyses, captured a variety of scenarios: cells resting on the glass substrate, cells being aspirated by the micropipette, and the micropipette itself in various orientations. The software's primary purpose is to continuously infer the positions of cells in the images (identified with the label *Cell*), the aspirated cell portion outside the micropipette (*Aspirated cell*), and the aspirated cell portion inside the micropipette (*Cell inside*). Figure 1 illustrates the labeling of images of two types, which is performed with polygons for the three types of objects inferred.

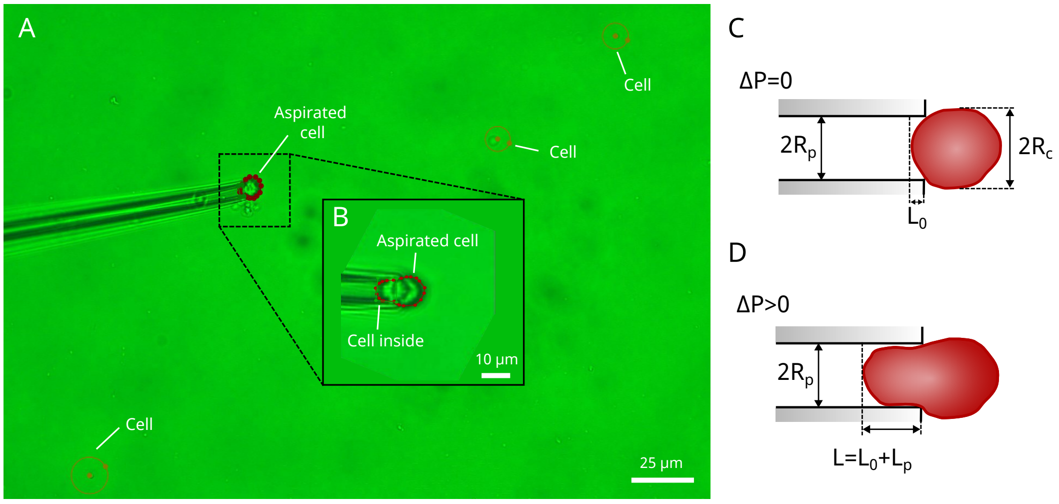

Figure 1: Examples of images used for training and validation of the artificial intelligence model for cell mechanical characterization in micropipette aspiration assays. (*A*) Complete image obtained in an assay. (*B*) Cropped and rotated region of interest, by the software developed in this work. The identified objects are labeled in both images. (*C,D*) Schemes showing the geometrical parameters extracted by the automatic analysis based on the AI tool: initial radius of the cell R_0 and aspirated length L_p. The internal radius of the micropipette, R_p is also used in the computations.

Cite as: Abarca-Ortega A, González-Bermúdez B, Plaza GR, Enhancing micropipette aspiration with artificial-intelligence analysis, Biophysical Journal, Volume 123, Issue 17, 2024, Pages 2860-2868,ISSN 0006-3495, DOI: https://doi.org/10.1016/j.bpj.2024.04.006.

Training and validation data

The curated dataset, split into 70% (168 images) for training and 30% (71 images) for validation, captures various cell scenarios in micropipette aspiration assays. The dataset was annotated using the open-source software `LabelMe` (CSAIL-MIT, USA). Individual polygons were meticulously drawn to delineate the three object types of interest for inference: cells, aspirated cells, and the micropipette. These annotations were then exported as JSON files containing the object coordinates.

Neural Network

With the training and validation image sets, we configured the model for training using a *Single Shot Multibox Detector* (SSD) architecture. This framework facilitates rapid object inference, faster than other two-stage detectors. It directly predicts object class and bounding boxes from feature maps (17). Feature extraction employed *EfficientNet-B0* and *Bidirectional Feature Pyramid Network* (BiFPN) to capture relevant features of the object, allowing effective image classification and combination of object features at different scales. This backbone network extracts relevant features from the input image using a series of convolutional layers with inverted bottlenecks. Its architecture balances accuracy and efficiency, making it suitable for resource-constrained environments (18, 19). BiFPN enhances feature representation by combining information from multiple scales within the feature pyramid. It allows for effective fusion of high-level semantic features with fine-grained details, improving both object detection and classification (19). The model aims to recognize three different classes in high-resolution images. The SSD model consists of several essential layers. The feature extraction layer employs the EfficientNet-B0 network with Bifpn. It utilizes a SWISH activation function and batch normalization with a controlled decay rate (0.99). The Bifpn layer is configured with a minimum and maximum level of 3 and 7, respectively, and undergoes three iterations with 64 filters. Transfer learning was employed, utilizing the pre-trained *EfficientDet-D0* model (18) on the COCO dataset (20). This model served as a starting point, including the ability to identify low-level features such as textures and edges. The choice of *EfficientDet-D0* was based on its efficiency, fast inference and training, and lower computational cost. The model was configured to process images of 2048x1536 pixels, and its parameters were adjusted for optimal learning.

The training configuration included the following parameters: (a) training for 10,000 epochs, where each epoch represents a model training update to refine neural network weights. (b) Batch of size 2, processing two training images simultaneously, optimized for computational cost. (c) Maximum number of box set to 100, limiting the total number of objects to detect in a single image. (d) Random horizontal flipping to create rotated versions of training images, enhancing model robustness. (e) Evaluation with batch size 1 to assess the model and calculate its accuracy on individual images. These choices balanced accuracy, training speed, resource utilization, and generalization capabilities. All configuration parameters, training and validation images, checkpoints, and the generated model can be found in the code repository for this study (21). The training and validation procedures were implemented using open-source code in `Python 3.11`, leveraging deep learning libraries such as `Keras` and `Tensorflow 2.0` (22, 23),and executed on the `Google Colab` platform for collaborative cloud programming.

Model Evaluation

Within the context of our object detection model based on SSD with the EfficientNet-B0 network, fundamental metrics are employed during the training process to assess model performance. The total loss serves as a global metric, combining classification loss, localization loss, and regularization loss through a weighting of their respective coefficients. Classification loss measures the discrepancy between predicted and actual classes, while localization loss evaluates accuracy in predicting bounding box coordinates. Regularization loss, implemented as an L2 penalty, contributes to model stability. Localization loss is computed using a Smooth L1 Loss function. The total loss is computed by summing these individual losses with appropriate weighting. The learning rate, a critical parameter in model training, follows a cosine decay throughout the process. Initially set at 0.005, the learning rate gradually decreases to 0.001 in the first 2500 warm-up steps, after which it remains constant. This cosine decay approach facilitates more precise and stable model convergence. Visualization and analysis of these metrics during training are conducted through `TensorBoard` platform.

Analysis of experiments

After successfully generating the AI model and ensuring accurate inferences on cell images, an image analysis code was developed to extract mechanical properties from cells in micropipette aspiration experiments. This processing code is broken

Cite as: Abarca-Ortega A, González-Bermúdez B, Plaza GR, Enhancing micropipette aspiration with artificial-intelligence analysis, Biophysical Journal, Volume 123, Issue 17, 2024, Pages 2860-2868,ISSN 0006-3495, DOI: https://doi.org/10.1016/j.bpj.2024.04.006.

down into seven key stages. In the first stage, the AI model is employed to infer the position of the cell to be aspirated in the initial raw image of the experiment. The center of this cell is taken as the center of a region of interest which is then cropped. Additionally, this new center serves as a pivot for rotating the image until the pipette becomes horizontal with the cell about to be aspirated to the right side (stage 2) (see Figure 1). The rotation angle and cropping coordinates are determined in this stage and applied to the entire sequence of images. Subsequently, in stage 3, the cell radius R_c is estimated and the position of the cell in the sequence of cropped and rotated images is inferred. The stage 4 involves measuring the aspiration length, L_p, inside the micropipette by tracking the left part of the cell's inference box (the cell front). With this information and the known size of the pipette R_p (5 μm) (stage 5), the normalized aspirated length L_p/R_p, is calculated. From the experiment data, the differential aspiration pressure at each moment, ΔP, is obtained (stage 6). Finally, in the stage 7, the aspiration curve, L_p/R_p vs ΔP, is generated, and a linear fit with the model presented in Equation 1 is performed in the range between 0.1 and 0.3 of the normalized aspirated length to obtain the Young's modulus E. This process is repeated for all the tests, being entirely automated and executed online, eliminating any delays in supervised analysis. The post-processing software is implemented using the `Python` programming language. Figure 2 illustrates the complete process of generating the AI model for cell identification, as well as the sequential steps of the analysis software, allowing computing mechanical parameters.

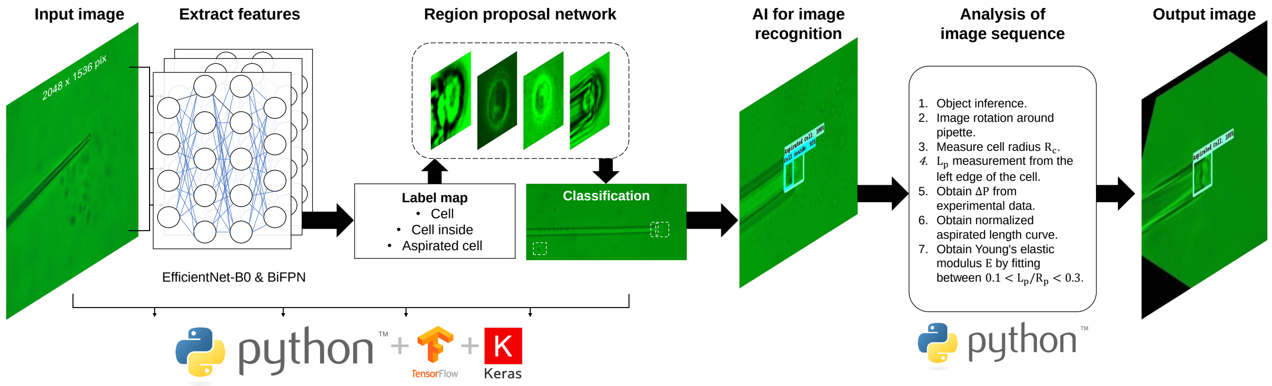

Figure 2: Scheme of the process of generation of the AI model, and its application to analysis of experiments.

RESULTS

In this section we describe the results of the AI model training and efficiency analysis. The model is applied to analyze micropipette-aspiration experiments of T cells.

Neural network training

A neural network was developed for analyzing images of micropipette aspiration experiments. Four iterations of the neural network model training were executed; in each one of them the architecture parameters were adjusted to optimize the process. Regarding the model architecture, a carefully selected combination of components was chosen to optimize object detection in high-resolution images. The SSD model was chosen for its ability to perform rapid inferences, eliminating the need for separate region proposal stages (17). Feature extraction was performed using EfficientNet-B0 and BiFPN, allowing the capture of relevant object features and the fusion of information from multiple scales in the feature pyramid, enhancing both object detection and classification. Special emphasis was placed on the choice of EfficientDet-D0 as a pre-trained model, due to its efficiency, training and inference speed, and lower computational cost (18, 19). Furthermore, the model's parameters were adjusted to optimize its performance on our data, including batch size, maximum number of boxes and activation function. These adjustments were made with a balance between accuracy, training speed, resource utilization, and the model's generalization capabilities in mind (19). Compared to other approaches such as Convolutional Regional Detectors (R-CNN) or Pyramid-based Detectors (P-RCNN), the SSD architecture offers a significant advantage in terms of inference speed and design simplicity, resulting in better performance in real-time scenarios and resource-limited environments (24). Compared with other pre-trained object detection architectures such as Faster R-CNN or You Only Look Once (YOLO) (25), EfficientDet-D0 offers an optimal balance between accuracy and computational efficiency, making it particularly suitable for applications in resource-limited environments or with processing time constraints (26, 27).

Cite as: Abarca-Ortega A, González-Bermúdez B, Plaza GR, Enhancing micropipette aspiration with artificial-intelligence analysis, Biophysical Journal, Volume 123, Issue 17, 2024, Pages 2860-2868,ISSN 0006-3495, DOI: https://doi.org/10.1016/j.bpj.2024.04.006.

Several metrics were employed to assess the performance and accuracy of the generated model, indicating its performance during training and facilitating parameter adjustments for further iterations. The metrics utilized include the total loss, localization loss, regularization loss, and learning rate (28–30). These key training metrics are depicted in Figure 3, plotted as a function of the total number of training steps. Figure 3A shows the progression of total loss, representing the error in identifying objects of interest (cells).

The gradual decrease in this value indicates a progressive improvement. Localization loss, quantifying the object localization error, is displayed in Figure 3B, showing a similar progressive reduction. The low values achieved for these parameters guarantee the convergence of the neural network training. The last two metrics, regularization loss and learning rate, serve as indicators of correct training, preventing overfitting issues (22). Figure 3C shows the evolution of regularization loss, indicating whether the neural network becomes too specialized with training data and loses generalization ability. Monitoring this metric ensures it remains consistently low, avoiding overfitting. Last, Figure 3D shows the model's learning rate, controlling how much the convolutional neural network weights are adjusted during training to minimize losses. The decreasing learning rate corresponds to low model losses, signaling a suitable point to conclude training (23). Considering these metrics, particularly the model's efficiency, the generated neural network exhibits a total loss of only 0.09 (see Figure 3.A). This value indicates a relatively low error between the model's predictions and actual values, i.e. a good efficiency.

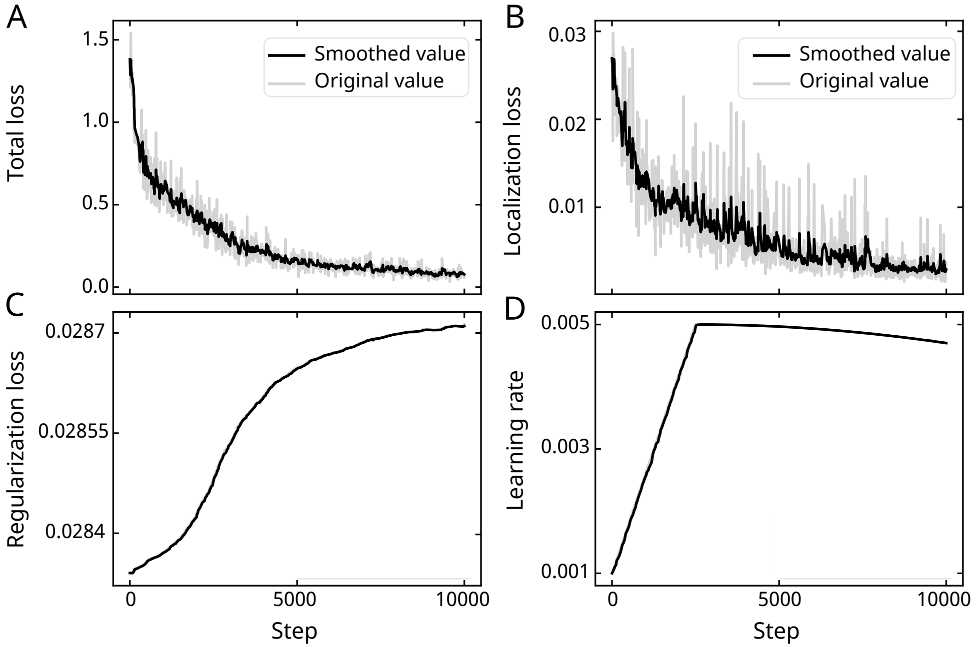

Figure 3: Results of neural network training for cell detection in micropipette aspiration assay images. (*A*) Total loss, (*B*) localization loss, (*C*) regularization loss, and (*D*) learning rate, plotted against the number of training steps. Exponential smoothing was applied to the original curves for better visualization.

Figure 3C shows a slight increase in the loss of regularization observed during CNN training, which may seem counterintuitive. Regularization techniques are commonly employed to prevent overfitting and improve the model's generalization to unseen data. One possible explanation for this escalation in regularization loss could be the growing complexity of the model, as it learns additional features from the training data. Although this complexity may enhance performance on the training set, it could potentially lead to poorer performance on the test set. Alternatively, it is plausible that adjustments to the regularization hyperparameters are necessary to optimize the model performance. It is essential to acknowledge that other vital metrics, such as training loss and validation accuracy, continued to exhibit improvement throughout the training process. This shows that, although regularization loss may increase, the model's ability to generalize to new data could still be progressing positively.

Once generated the neural-network model by training, as explained, a code was implemented for model application, conducting inference on each assay image to measure cell movement within the pipette during aspiration. By this procedure,

Cite as: Abarca-Ortega A, González-Bermúdez B, Plaza GR, Enhancing micropipette aspiration with artificial-intelligence analysis, Biophysical Journal, Volume 123, Issue 17, 2024, Pages 2860-2868,ISSN 0006-3495, DOI: https://doi.org/10.1016/j.bpj.2024.04.006.

the advance of the cell front was measured for each image (see Supplementary videos 1 and 2). Besides, for each image the aspiration pressure was recorded during the experiment. The code automatically adjusts image analysis results to Zhou's linearized model (11), yielding the apparent Young's elastic modulus for each cell. With our code, the entire analysis process for a set of experiments is automated, with the user only required to specify the directory containing the images of the experiments. The code can be found in the virtual repository for this study (21).

Comparison with other analysis techniques

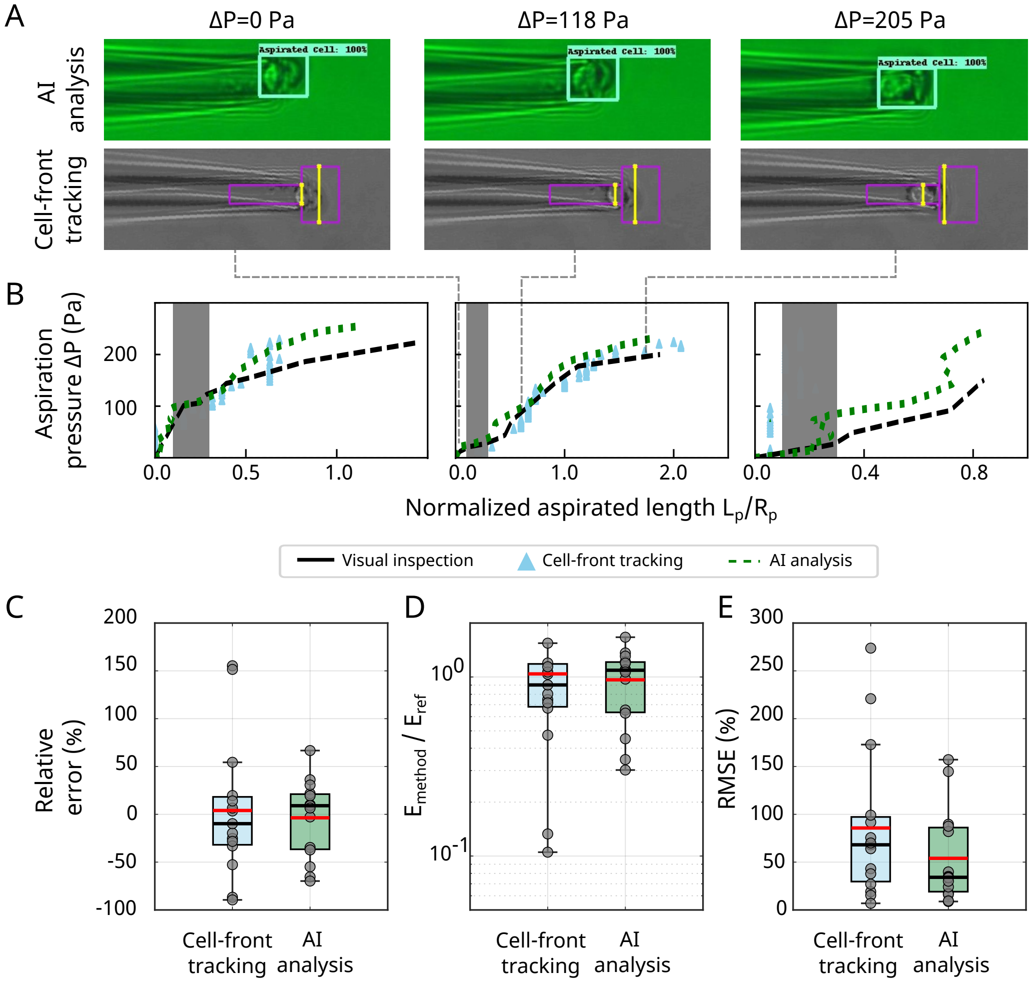

Figure 4: Comparison of experiment analysis by visual inspection (taken as reference), by unsupervised automatic cell-front tracking and by the AI tool. (*A*) Representative images of an aspiration experiment and the regions of interest identified in the two automatic methods: cell-front tracking and AI tool. (*B*) Three examples showing the values of the aspirated length L_p normalized by the pipette radius R_p (horizontal axis), as estimated by the three techniques: visual inspection and tracking performed by the user, unsupervised cell-front tracking code, and AI analysis. The data in the interval between $L_p/R_p = 0.1$ and 0.3, in grey color, are used for the linear fit to estimate the apparent Young's modulus. The vertical axis shows the aspiration pressure ΔP. (*C*) Relative error of the estimated apparent Young's modulus using unsupervised methods (cell-front tracking and AI analysis), with respect to the visual-inspection method obtained manually. (*D*) Ratio between the estimated apparent Young's modulus using unsupervised methods (cell-front tracking and AI analysis), represented in logarithmic scale (*E*) Root mean squared error obtained for the complete set of values L_p/R_p in the curves (whole curve) for both inspection techniques compared to that obtained manually. The values were computed for 15 experiments.In (*C*-*E*), the red solid line is the mean and the black solid line is the median.

Cite as: Abarca-Ortega A, González-Bermúdez B, Plaza GR, Enhancing micropipette aspiration with artificial-intelligence analysis, Biophysical Journal, Volume 123, Issue 17, 2024, Pages 2860-2868,ISSN 0006-3495, DOI: https://doi.org/10.1016/j.bpj.2024.04.006.

To assess the accuracy of the mechanical characterization of cells using the generated neural network, various image analysis techniques were compared for a set of previously performed experiments, which were not part of the model training data set (the micropipette aspiration technique is described in other articles of our group (7, 11, 12)). We compared the results obtained (a) by visual image analysis based on cell edge tracking using `ImageJ` software, (b) by using a previously employed `Matlab` code (12), which tracks the cell front during the aspiration experiment by detecting a threshold in pixel intensity and requires extensive user interaction but which was run without supervision for the purpose of this comparison, and (c) by using the neural network. The three methods allow assessing the aspirated length, L_p, of the cell, i.e. the distance between the cell front and its position when the cell in unloaded. This aspirated length has been used to compute the Young's modulus by using the linear equation described in 'Materials and Methods' section (11).

For this comparison, 15 experiments were randomly selected from previously conducted experiments (12), and all three analysis techniques were applied to each experiment (see Figure S1 and Table S1 in Supplementary Information). The results are shown in Figure 4. The visual image analysis technique by using `ImageJ`, in which the user manually selects measurement points in each image, was chosen as the reference. For this work, the automated cell tracking results provided by the other two techniques were used to compute the apparenet Young's modulus by means of unsupervised routines.

The comparison of the three techniques applied to image analysis (see Figure 4B reveals similar cell-front tracking in almost all analyzed experiments. Figure 4C shows the relative error in the estimation of the apparent Young's modulus compared to the visual inspection method, taken as a reference. Although the cell-front tracking analysis code allows the user to assess the edge detection effectiveness, enabling the exclusion of Young's modulus values when the edge detection error is glaringly evident, here we have used the cell-tracking code in an unsupervised way for the comparison with the also unsupervised methodology to compute the Young's apparent modulus using the AI tool. As a result, the median deviation in Young's modulus calculation with this code is -9.8% and the mean is 4.0% . With a high number of experiments and a supervised methodology to disregard values when the edge detection is poorly executed, the average error of the code is negligible (12, 31). For Young's modulus calculations using the neural network, the median deviation is 9% and the mean is -3.6%, with the advantage of being more robust. Figure 4D shows the ratio between the apparent Young's modulus calculated by the unsupervised methods as compared with the visual-inspection method. The cell-tracking method yields a mean ration of 1.039 and median of 0.902, while the AI tool provides similar values, with mean 0.964.

Figure 4E shows the root-mean-square error (RMSE) of the complete curves for each technique compared to manual visual inspection. This metric serves as an indicator of the error in curve prediction obtained through image analysis techniques. The median RMSE is approximately double for the cell-front tracking technique (68%) compared to that of the AI tool (34%), while the mean RMSE is also higher (86%) in the cell-front tracking method than in the AI method (54%). Consequently, the artificial intelligence technique consistently outperforms the former in cell tracking accuracy.

The analysis conducted on 15 experiments provides insight into the magnitude of the error introduced by the two automated analysis techniques for estimating the apparent Young's modulus of cells. Both techniques yield Young's modulus values of the same order of magnitude as those obtained through direct visual inspection by the researcher. We believe that these methods are suitable for detecting significant differences between cell populations. In its current implementation, the use of the neural network allows for robust estimations, as demonstrated in the analysis. Future enhancement of the training image library may further reduce the deviation from estimates made through direct visual inspection of images.

DISCUSSION

The analysis conducted on 15 experiments provides insight into the magnitude of the error introduced by the two automated analysis techniques for estimating the apparent Young's modulus of cells. Both techniques yield Young's modulus values of the same order of magnitude as those obtained through direct visual inspection by the researcher. We believe that these methods are suitable for detecting significant differences between cell populations. In its current implementation, the use of the neural network allows for robust estimations, as demonstrated in the analysis. Future enhancement of the training image library may further reduce the deviation from estimates made through direct visual inspection of images. Our results highlight the effectiveness of the artificial intelligence model implementation, despite having a relatively small dataset. This effectiveness is reflected in the robustness and efficacy of our approach, particularly in the context of T cells. Although the dataset size may seem limited for training a traditional CNN robustly, the results obtained suggest it was sufficient for our specific application. Tracking the entire process of cell aspiration, as opposed to solely at relatively small deformations, can be very important when

Cite as: Abarca-Ortega A, González-Bermúdez B, Plaza GR, Enhancing micropipette aspiration with artificial-intelligence analysis, Biophysical Journal, Volume 123, Issue 17, 2024, Pages 2860-2868,ISSN 0006-3495, DOI: https://doi.org/10.1016/j.bpj.2024.04.006.

considering large deformation and viscoelastic effects experienced when the cell undergoes substantial deformations over an extended time (32). Therefore, using artificial intelligence to apply hyperelasticity or viscoelasticity models promises more efficient and accurate assessment of mechanical measurements in the long run.

The most impressive difference is obtained when comparing the time required for the researcher to compute Young's moduli of cells in a set of experiments. The use of the neural network is purely automatic and therefore the time required for the user is negligible. By contrast, in the case of visual inspection, the time required to analyze one experiment, measuring L_p on various images, is of the order of 10 minutes, and the use of the cell-front tracking code requires approximately 5 minutes for experiment, taking into account the visual validation of the user. Therefore, for instance, 100 experiments would require around eight hours for the visual-inspection method and around four hours by using the cell-front tracking code, compared to the purely automated analysis by using the neural network.

The results of the neural network training for micropipette aspiration experiments demonstrated promising outcomes. The network exhibited efficient learning, as indicated by the progressively decreasing total loss and localization loss metrics during training (Figure 3). The low regularization loss and appropriate learning rate further underscored the avoidance of overfitting, ensuring the generalization ability of the neural network. The 0.09 performance achieved by the automated image analysis software reflects the model's capability to recognize and locate objects of interest accurately. The comparison with other image analysis techniques, including the previously utilized `Matlab` code and manual analysis using `ImageJ`, showcased the robustness of the neural network approach. The deviations observed in Young's modulus calculations using the neural network were comparable to or even lower than those of traditional methods. The ability to perform fully automated analyses without user bias is a significant advantage. Moreover, the neural network demonstrated higher resilience to extreme errors compared to the `Matlab` code, ensuring more reliable and consistent results.

While the neural network model proved effective, it is not without limitations. Further refinement of the model architecture and careful adjustment of training methods may enhance its performance, mitigating potential overfitting issues. Expansion of the labeled image dataset, including diverse cell types and pipette geometries, could improve the model's robustness and broaden its applicability. The development of a generalist neural network capable of detecting various aspirated materials, such as organs or fungi, represents an intriguing avenue for future research. The comparison with traditional techniques emphasizes the potential of the automated image analysis software to streamline and improve micropipette aspiration experiments. The discrepancy in Young's modulus calculations can be attributed to the inherent differences in manual and automated tracking methods, highlighting the need for standardization in biomechanical analyses. The neural network, despite its current limitations, presents a compelling alternative for reliably characterizing cell mechanics, paving the way for more extensive and consistent experimental studies.

The automated image analysis software, driven by a well-trained neural network, provides a robust and user-friendly platform for micropipette aspiration experiments. The comparison with traditional techniques underscores its effectiveness and potential for advancing biomechanical analyses. Future work should focus on refining the neural network model and expanding the dataset, opening avenues for broader applications in cell mechanics and material aspiration studies. The incorporation of artificial intelligence enables the efficient handling of large-scale experiments, facilitating the identification of significant differences in cell mechanical properties across various conditions. Furthermore, the approach offers the possibility of performing real-time measurements of mechanical properties, a capability with applications such as cell sorting and selection.

CONCLUSION

The integration of artificial intelligence tools in mechanobiology holds tremendous potential for expanding experimental capacities in laboratories. In this study, a neural network-based code was developed for the automated analysis of micropipette aspiration assay images. The training and analysis methodology proved effective, showcasing a robust model capable of recognizing and localizing objects with high precision. The neural network achieved an impressive performance in automated image recognition, providing a valuable tool for unbiased, cloud-compatible, and user-friendly analysis of cell deformation during micropipette aspiration experiments. Comparisons with other image analysis techniques demonstrated the new software's robustness and efficacy, positioning it as a suitable method for detecting significant differences between cell samples.

Certain limitations merit consideration. The neural network introduced a margin of error in calculating Young's modulus. Future improvements could involve careful fine-tuning of the deep learning model to expand the labeled image dataset used

Cite as: Abarca-Ortega A, González-Bermúdez B, Plaza GR, Enhancing micropipette aspiration with artificial-intelligence analysis, Biophysical Journal, Volume 123, Issue 17, 2024, Pages 2860-2868,ISSN 0006-3495, DOI: https://doi.org/10.1016/j.bpj.2024.04.006.

for training, including diverse cell types and aspiration device geometries to enhance model robustness. Additionally, future research could explore the development of a generalized neural network model capable of detecting various aspirated materials, extending the tool's applicability to a broader range of experiments. Furthermore, we are working on generalizing the software to accommodate different types of cells and tissues, opening up new possibilities for real-time application in a variety of biological materials. In conclusion, while the study has unveiled a powerful AI-based tool for micropipette aspiration analysis, ongoing refinement and exploration of new applications remain integral for advancing this field.

AUTHOR CONTRIBUTIONS

A.A-O. and B.G-B. performed the labeling and preprocessing of the images, A.A-O. and G.P. set up the CNN training structure and procedure, A.A-O. and B.G-B. performed the experimental tests and comparison of techniques. All authors contributed to the design of the paper and the writing of the article.

ACKNOWLEDGMENTS

The authors received support from the Comunidad de Madrid, Spain, projects Tec4Bio-CM/P2018/NMT-4443 and MINA-CM S2022-BMD-7236. In addition, A.A-O. thanks the support provided by DICYT from the Universidad de Santiago de Chile and by ANID PFCHA/DOCTORADO BECAS CHILE/2019 – CEL00011051, and to the Faculty of Engineering (FING) USACH.

DECLARATION OF INTERESTS

The authors declare no competing interests.

REFERENCES

1. Carlo, D. D., 2012. A Mechanical Biomarker of Cell State in Medicine. *Journal of Laboratory Automation* 17:32–42. https://doi.org/10.1177/2211068211431630.

2. Teck LIM, C., 2006. Single Cell Mechanics Study of the Human Disease Malaria *. *Journal of Biomechanical Science and Engineering* 1.

3. González-Bermúdez, B., A. Abarca-Ortega, M. González-Sánchez, M. D. la Fuente, and G. R. Plaza, 2022. Possibilities of using T-cell biophysical biomarkers of ageing. *Expert Reviews in Molecular Medicine* 24. https://doi.org/10.1017/erm.2022.29.

4. Urbanska, M., H. E. Muñoz, J. Shaw Bagnall, O. Otto, S. R. Manalis, D. Di Carlo, and J. Guck, 2020. A comparison of microfluidic methods for high-throughput cell deformability measurements. *Nature Methods* 17:587–593.

5. Abarca-Ortega, A., B. González-Bermúdez, C. Castro-Domínguez, A. Álvarez López, C. Díaz-Alcaraz, M. Garvía-Rodríguez, G. V. Guinea, and G. R. Plaza, 2024. Single-cell mechanical characterization in constriction-based cytometry. *International Journal of Mechanical Sciences* 268:108979. https://www.sciencedirect.com/science/article/pii/S0020740324000225.

6. Mitchison, J. M., and M. M. Swann, 1954. The Mechanical Properties of the Cell Surface: I. The Cell Elastimeter. *Journal of Experimental Biology* 31:443–460. https://doi.org/10.1242/jeb.31.3.443.

7. González-Bermúdez, B., G. V. Guinea, and G. R. Plaza, 2019. Advances in Micropipette Aspiration: Applications in Cell Biomechanics, Models, and Extended Studies. *Biophysical Journal* 116:1–16. https://doi.org/10.1016/j.bpj.2019.01.004.

8. González-Bermúdez, B., H. Kobayashi, Á. Navarrete, C. Nyblad, M. González-Sánchez, M. de la Fuente, G. Fuentes, G. V. Guinea, C. García, and G. R. Plaza, 2020. Single-cell biophysical study reveals deformability and internal ordering relationship in T cells. *Soft Matter* .

9. Trickey, W. R., G. M. Lee, and F. Guilak, 2000. Viscoelastic properties of chondrocytes from normal and osteoarthritic human cartilage. *Journal of Orthopaedic Research* 18:891–898. https://doi.org/10.1002/jor.1100180607.

Cite as: Abarca-Ortega A, González-Bermúdez B, Plaza GR, Enhancing micropipette aspiration with artificial-intelligence analysis, Biophysical Journal, Volume 123, Issue 17, 2024, Pages 2860-2868,ISSN 0006-3495, DOI: https://doi.org/10.1016/j.bpj.2024.04.006.

10. Theret, D. P., M. J. Levesque, M. Sato, R. M. Nerem, and L. T. Wheeler, 1988. The Application of a Homogeneous Half-Space Model in the Analysis of Endothelial Cell Micropipette Measurements. *Journal of Biomechanical Engineering* 110:190–199. https://doi.org/10.1115/1.3108430.

11. Plaza, G. R., T. Q. P. Uyeda, Z. Mirzaei, and C. A. Simmons, 2015. Study of the influence of actin-binding proteins using linear analyses of cell deformability. *Soft Matter* 11:5435–5446. https://doi.org/10.1039/c5sm00125k.

12. Esteban-Manzanares, G., B. González-Bermúdez, J. Cruces, M. D. la Fuente, Q. Li, G. V. Guinea, J. Pérez-Rigueiro, M. Elices, and G. R. Plaza, 2017. Improved Measurement of Elastic Properties of Cells by Micropipette Aspiration and Its Application to Lymphocytes. *Annals of Biomedical Engineering* 45:1375–1385. https://doi.org/10.1007/s10439-017-1795-7.

13. Zhou, E. H., C. T. Lim, and S. T. Quek, 2005. Finite Element Simulation of the Micropipette Aspiration of a Living Cell Undergoing Large Viscoelastic Deformation. *Mechanics of Advanced Materials and Structures* 12:501–512. https://doi.org/10.1080/15376490500259335.

14. Berardi, M., K. Bielawski, N. Rijnveld, G. Gruca, H. Aardema, L. van Tol, G. Wuite, and B. I. Akca, 2021. Optical interferometry based micropipette aspiration provides real-time sub-nanometer spatial resolution. *Commun Biol* 4:610.

15. González-Bermúdez, B., H. Kobayashi, A. Abarca-Ortega, M. Córcoles-Lucas, M. González-Sánchez, M. D. la Fuente, G. V. Guinea, M. Elices, and G. R. Plaza, 2022. Aging is accompanied by T-cell stiffening and reduced interstitial migration through dysfunctional nuclear organization. *Immunology* 167:622–639. https://doi.org/10.1111/imm.13559.

16. Guck, J., 2019. Some thoughts on the future of cell mechanics. *Biophysical Reviews* 11:667–670.

17. Liu, W., D. Anguelov, D. Erhan, C. Szegedy, S. Reed, C.-Y. Fu, and A. C. Berg, 2016. SSD: Single Shot MultiBox Detector. *In* Computer Vision – ECCV 2016, Springer International Publishing, 21–37. https://doi.org/10.1007/978-3-319-46448-0_2.

18. Tan, M., R. Pang, and Q. V. Le, 2020. EfficientDet: Scalable and Efficient Object Detection. *In* 2020 IEEE/CVF Conference on Computer Vision and Pattern Recognition (CVPR). IEEE. https://doi.org/10.1109/cvpr42600.2020.01079.

19. Zhu, L., Z. Deng, X. Hu, C.-W. Fu, X. Xu, J. Qin, and P.-A. Heng, 2018. Bidirectional Feature Pyramid Network with Recurrent Attention Residual Modules for Shadow Detection. *In* Computer Vision – ECCV 2018, Springer International Publishing, 122–137. https://doi.org/10.1007/978-3-030-01231-1_8.

20. Lin, T.-Y., M. Maire, S. Belongie, J. Hays, P. Perona, D. Ramanan, P. Dollár, and C. L. Zitnick, 2014. Microsoft COCO: Common Objects in Context. *In* Computer Vision – ECCV 2014, Springer International Publishing, 740–755. https://doi.org/10.1007/978-3-319-10602-1_48.

21. Abarca-Ortega, A., 2023. Github Repository - Micropipette aspiration IA. https://github.com/AspirationTeamCTB-UPM/Micropipette_aspiration_IA. [Accessed 23-Nov-2023].

22. Gulli, A., A. Kapoor, and S. Pal, 2019. Deep Learning with TensorFlow 2 and Keras. Packt Publishing, Birmingham, England, 2 edition.

23. Abadi, M., P. Barham, J. Chen, Z. Chen, A. Davis, J. Dean, M. Devin, S. Ghemawat, G. Irving, M. Isard, et al., 2016. Tensorflow: A system for large-scale machine learning. *In* 12th {USENIX} Symposium on Operating Systems Design and Implementation ({OSDI} 16). 265–283.

24. Ren, S., K. He, R. Girshick, and J. Sun, 2017. Faster R-CNN: Towards Real-Time Object Detection with Region Proposal Networks. *IEEE Transactions on Pattern Analysis and Machine Intelligence* 39:1137–1149. http://dx.doi.org/10.1109/TPAMI.2016.2577031.

25. Redmon, J., S. Divvala, R. Girshick, and A. Farhadi, 2016. You Only Look Once: Unified, Real-Time Object Detection. *In* 2016 IEEE Conference on Computer Vision and Pattern Recognition (CVPR). IEEE. http://dx.doi.org/10.1109/CVPR.2016.91.

26. Sasirekha, R., J. Jeyshri, A. TinaVictoria, J. Subha, and P. Kamaleswari, 2023. Review on Deep Learning Algorithms for Object Detection, Springer Nature Singapore, 421–428. http://dx.doi.org/10.1007/978-981-99-1726-6_32.

Cite as: Abarca-Ortega A, González-Bermúdez B, Plaza GR, Enhancing micropipette aspiration with artificial-intelligence analysis, Biophysical Journal, Volume 123, Issue 17, 2024, Pages 2860-2868,ISSN 0006-3495, DOI: https://doi.org/10.1016/j.bpj.2024.04.006.

27. Sanchez, S. A., H. J. Romero, and A. D. Morales, 2020. A review: Comparison of performance metrics of pretrained models for object detection using the TensorFlow framework. *IOP Conference Series: Materials Science and Engineering* 844:012024. `http://dx.doi.org/10.1088/1757-899X/844/1/012024`.

28. Girshick, R. B., 2015. Fast R-CNN. *CoRR* abs/1504.08083. `http://arxiv.org/abs/1504.08083`.

29. Chollet, F., 2017. Deep Learning with Python. Manning.

30. Krizhevsky, A., I. Sutskever, and G. E. Hinton, 2017. ImageNet classification with deep convolutional neural networks. *Communications of the ACM* 60:84–90. `http://dx.doi.org/10.1145/3065386`.

31. González-Bermúdez, B., 2021. Deformability of T cells as a mechanical biomarker of immunosenescence and development of techniques for the clinical application. Ph.D. thesis, UPM - E.T.S.I. Caminos, Canales y Puertos. `https://doi.org/10.20868/upm.thesis.69384`.

32. Plaza, G. R., N. Marí, B. G. Gálvez, A. Bernal, G. V. Guinea, R. Daza, J. Pérez-Rigueiro, C. Solanas, and M. Elices, 2014. Simple measurement of the apparent viscosity of a cell from only one picture: Application to cardiac stem cells. *Physical Review E* 90. `https://doi.org/10.1103/physreve.90.052715`.

SUPPLEMENTARY MATERIAL

The supplementary material contains the results of the 10 random comparisons performed with the three image analysis techniques for experimental characterization of cells by micropipette aspiration, and two representative videos. In addition, the generated artificial intelligence tool and the code for mechanical characterization are available in the repository: `https://github.com/AspirationTeamCTB-UPM/Micropipette_aspiration_IA`.